The diffusion limit of ballistic transport in the scrape-off layer

P. Manz[1,2], C. Hufnagel[2,1], A. Zito[3,1], D. Carralero[4], M. Griener[1], T. Lunt[1], O. Pan[1]. M. Passoni[3], B. Tal[1], M. Wischmeier[1], E. Wolfrum[1] and the ASDEX Upgrade Team[a]

[1] *Max Planck Institute for Plasma Physics, Boltzmannstr.2 ,85748 Garching, Germany*

[2] *Physik-Department E28, Technische Universität München, 85748 Garching, Germany*

[3] *Dipartimento di Energia, Politecnico di Milano, Via Ponzio 34/3, 20133 Milano, Italia*

[4] *Laboratorio Nacional de Fusión, CIEMAT, 28040 Madrid, Spain*

[a] *see the author list of H.Meyer et al. 2019 Nucl.Fusion 59 112014*

(Dated: October 14, 2019)

Abstract

At least in the far scrape-off layer of magnetically confined fusion plasmas transport is intermittent and non-diffusive as observed by the appearance of plasma filaments. Transport codes using effective diffusion coefficients are still the main workhorse investigating the scrape-off layer and divertor regions. An effective perpendicular diffusion coefficient for intermittent filamentary dominated perpendicular transport in the scrape-off layer is motivated by the telegraph equation, describing an exponentially decaying correlated random walk. On short time scales the telegraph equation describes ballistic transport of filamentary structures with a typical velocity u_b and correlation time τ. In stationary conditions the corresponding diffusion coefficient is given by $u_b^2\tau$. Since u_b and τ can be determined experimentally it is proposed to use $u_b^2\tau$ as an input for modeling or for interpretation of perpendicular transport in the far scrape-off layer.

INTRODUCTION

A magnetically confined fusion plasma is surrounded by a region of open field lines intersecting on material surfaces. This region is called the scrape-off layer (SOL). It governs the heat load on the plasma facing components, the power and particle balance and the impurity dynamics. The SOL region can be further divided into two regions, a near and a far SOL [1]. The region close to the separatrix, called near SOL, exhibits gradient lengths close to those in the edge of the confined region. The much flatter SOL profile away from the separatrix is called the far SOL region. At least in the far SOL transport is determined to a huge fraction by intermittently occurring coherent structures of enhanced plasma pressure [2–5]. In the poloidal cross-section or drift-plane they appear compact and localized and are therefore called plasma blobs. These structures are also field-aligned [6] and therefore also called plasma filaments. Blobs are driven by the interchange instability [7, 8]. Due to these blobs the transport shows non-Gaussian statistics with exponential tails and hence is non-diffusive. Due to the rather flat gradients transport in the far SOL cannot be locally generated [9] and the observed high fluctuation levels are due to non-local transport [10].

Transport codes like SOLPS [11, 12], EDGE2D [13], EMC3 [14], UEDGE [15] or SOLedge2D [16] are still the main workhorses for interpretative and predictive studies in the scrape-off layer (SOL) and divertor region of magnetically confined fusion plasmas. These transport codes include atomic, molecular and plasma physical effects important for the SOL and divertor region, but they do not treat turbulence self-consistently. Instead the transport is approximated by spatially varying effective diffusion or convection coefficients. This leads to problems illustrated in the following in simplified geometry. The scrape-off layer in the poloidal cross-section of a tokamak is shown on the l.h.s. in Fig. 1. In this simplified geometry the scrape-off layer is straightened out as shown on the r.h.s. in Fig. 1. The straightened out scrape-off layer is bound by the opposite-facing solid surfaces (divertor targets or limiters) at the top and the bottom and to the left by the confined plasma. The problem reduces from three to two dimensions, the straightened out SOL exhibits a radial coordinate across the SOL and a coordinate parallel to the field lines (z) from the inner to the outer target. The evolution of the density in such a straightened out SOL can be provided by

$$\frac{\partial}{\partial t}n = D\frac{\partial^2}{\partial r^2}n - u_z\frac{\partial}{\partial z}n + S \tag{1}$$

using a diffusive ansatz for the perpendicular transport given by $\Gamma_{diff} = -D\frac{\partial}{\partial r}n$. This equation can be further simplified by approximating the parallel speed by the ion sound speed $u_\parallel \approx c_s$ and the parallel derivative by the parallel connection length $\frac{\partial}{\partial z} \approx 1/L_\parallel$. Neglecting sources and sinks, the gradient scale length $\lambda_n = -n/\frac{\partial}{\partial r}n$ can be approximated by

$$\lambda_n = \sqrt{DL_\parallel/c_s}. \tag{2}$$

For example in typical attached conditions in the near SOL ASDEX Upgrade tokamak $\lambda_n \sim 10^{-2}$ m, $c_s \sim 10^5$ m/s and $L_\parallel \sim 10^2$ m, hence $D \sim 10^{-1}$ m^2/s.

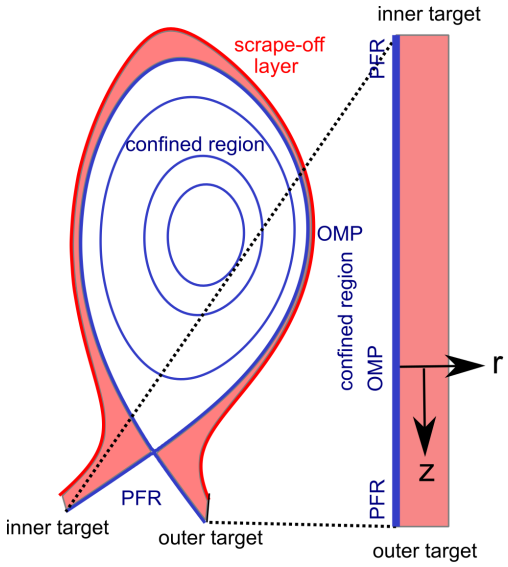

FIG. 1: The straightened out scrape-off layer concept. The private flux region is indicated by PFR, the outer midplane by OMP.

How to choose reasonable radial transport coefficients for the SOL? Bohm predicted a diffusion coefficient of $D_B \approx 0.06T_e/eB$, which only depends on magnetic field and temperature. The same holds for gyro-Bohm transport $D_{gB} = (\rho_s/\lambda_n)T_e/eB$ with $\rho_s = \sqrt{m_i T_e}/eB$. The density SOL length λ_n changes from about 10 mm in attached conditions up to 45 mm at the end of the formation of the density shoulder [17]. Assuming gyro-Bohm diffusion in this simple SOL model $T_e \sim \lambda_n^3$, a temperature increase by a factor 90 is needed to explain such a transition. However, experimentally the temperature is not found increasing nearly two orders of magnitude approaching detached conditions. Assuming the temperature unchanged in the simple SOL model, this corresponds to a difference of a factor of 20 in the corresponding diffusion coefficient.

To reproduce the shoulder formation in simulations an enhanced diffusion coefficients have to be assumed [18]. How can such a high diffusion coefficient be motivated? The broadening of λ_n is accompanied by a strong increase in filamentary transport [17, 19], which is mainly convective. Would a convective description of the SOL transport be more appropriate? In a convective ansatz the transport is given by $\Gamma_{\mathrm{conv}} = Un$. In a time independent approach diffusion and convection are formally exchangeable by defining $U = \sqrt{D_{\mathrm{diff}} c_s / L_{\parallel}}$. In this case convective and diffusive transport are equal $\Gamma_{\mathrm{conv}} = \Gamma_{\mathrm{diff}}$. Their combination seems to be described by convection or (preferred) diffusion only. Only a factor of four is needed in the convective velocity to explain the observed change in λ_n during the density ramp up, this factor of four is also observed in the experiment [20].

The radial velocity of the filaments ($u_b \sim$ 100 m/s to km/s) are much too high for effective convective velocities in the transport codes. The discrepancy is usually understood by the fact that the blobs appear only intermittently and not continuously in the time signal. Therefore, the filamentary transport should be weighted by the so-called blob packing fraction f_p (the blob frequency f_b times the auto-correlation time τ_b of the blobs). Using such a packing fraction the effective convective velocity is about two orders of magnitude lower than the typical filament velocity. Once the blob packing fraction and the filament velocity are known, the SOL length λ_n can be predicted [21]. Although the blob packing fraction provides means to obtain reasonable diffusion coefficients or effective convective velocities, there are at least two caveats using blob packing fractions. First, whereas the density transported by the filaments is reduced by the packing fraction, this approach reduces the speed $U = f_p u_b$) instead. Hence, the ratio of the time scales of the perpendicular and parallel dynamics are wrong. This intrinsically reduces the impact of the radial transport as the parallel dynamics has more time to deplete the density upstream. Second, the blob packing fraction depends on the blob generation process, which is highly non-linear and not understood well. One describes an unknown (perpendicular transport) by another unknown (blob packing fraction).

In the present contribution an effective diffusion coefficient describing non-diffusive filamentary transport in the SOL is motivated by the telegraph equation. The telegraph equation describes nonlocal, ballistic transport on the time scale of the plasma filaments and, as desired for transport codes, it provides a diffusive transport on equilibrium time scales. Furthermore, it is consistent with the correlation characteristics in the SOL. After

introducing the telegraph equation in Sec. , its dynamic features are illustrated in Sec. . An order of magnitude estimate of the effective diffusion coefficient is given in Sec. and an example of an application with the transport code SOLPS-ITER is shown in Sec. . Summary and conclusion are given in Sec. .

CORRELATION BASED DIFFUSION

Approaches to sub- and super-diffusion

In general turbulent transport is non-diffusive. In 1926 Richardson introduced the concept of anomalous diffusion to describe turbulent transport [22]. One way to describe anomalous diffusion is by generalized random walks, defined in terms of non- Gaussian jump and waiting time probability distributions. Unlike typical diffusion, where the mean square displacement scales linearly with time $\langle \Delta x \rangle^2 \sim Dt$, anomalous diffusion [23] differs from this linear scaling and $\langle \Delta x \rangle^2 \sim t^\nu$. In this generalized random walk framework the process is classified diffusive for $\nu = 1$, sub-diffusive for $\nu < 1$ and super-diffusive for $\nu > 1$. An alternative approach to anomalous diffusion is provided by a fractional diffusion equation $\frac{\partial^\beta}{\partial t^\beta} n = \frac{\partial^\alpha}{\partial x^\alpha} Dn$ where the parameters α and β do not have to be integers. The process can be classified by their ratio $\mu = \beta/\alpha$ and is diffusive for $\mu = 0.5$, sub-diffusive for $\mu < 0.5$ and super-diffusive for $\mu > 0.5$. Fractional diffusion has been studied in magnetically confined plasmas before [24–26], reduced resistive MHD turbulence has been shown to be super-diffusive [24], plasma core turbulence is close to diffusive, but becomes sub-diffusive in the presence of shear flows [26]. Where fractional calculus is interesting for interpretation, fractional derivatives are difficult to integrate in the numerical architecture of the already existing transport codes.

Concept of correlation based diffusion

A third concept of anomalous diffusion is correlation based diffusion [27]. From the continuity equation

$$\frac{\partial}{\partial t} n + u_r \frac{\partial n}{\partial r} = S \tag{3}$$

where the transport is represented by the second term on the l.h.s. and S represents possible sources and sinks. To study the impact of fluctuations, density and velocity are decomposed

in background and fluctuating quantities $n = n_0 + \tilde{n}$ and $u_r = u_{r0} + \tilde{u}_r$. In Ref. [27] the background is obtained by averaging $\langle\cdot\rangle$ the continuity equation over the ensemble of realizations. In the following, we will neglect the contribution of the background radial velocity u_{r0}, which is usually expected to be small in a tokamak. In the original work [27] the effect of u_{r0} can be found. The evolution of the background density is

$$\frac{\partial}{\partial t} n_0 = -\langle \tilde{u}_r \frac{\partial \tilde{n}}{\partial r} \rangle + S. \tag{4}$$

Turbulent transport $\Gamma = \langle \tilde{u}_r \tilde{n} \rangle$ is given by the second term. It does not vanish, if density and radial velocity fluctuations are correlated. The time evolution of the density perturbation is

$$\frac{\partial}{\partial t} \tilde{n} = -\tilde{u}_r \frac{\partial n_0}{\partial r}. \tag{5}$$

This equation can be solved by integration

$$\tilde{n}(x,t) = -\int_0^t \tilde{u}_r(t') \frac{\partial n_0}{\partial r} dt' \tag{6}$$

which can be inserted in the background equation (4)

$$\frac{\partial}{\partial t} n_0 = \int_0^t \langle \tilde{u}_r(t) \tilde{u}_r(t') \rangle \frac{\partial^2 n_0}{\partial r^2} dt' + S, \tag{7}$$

here

$$C(t,t') = \langle \tilde{u}_r(t) \tilde{u}_r(t') \rangle \tag{8}$$

is the auto correlation function of the radial velocity. Linear correlation can be represented by $C(t,t') = C(t-t')$. Therefore, transport depends on the auto-correlation function

$$\frac{\partial}{\partial t} n_0 = \frac{\partial^2 n_0}{\partial r^2} \int_0^t C(t-t') dt' + S. \tag{9}$$

The first term on the r.h.s. can be identified as the transport term

$$\frac{\partial}{\partial r} \Gamma = \frac{\partial^2 n_0}{\partial r^2} \int_0^t C(t-t') dt'. \tag{10}$$

Short- and long-time correlations

A different type of correlation function leads to a different transport phenomenology. In the case of short time correlation represented by the delta correlation function

$$C(t-t') = D_l \delta(t-t')$$

Eq. (9) reduces to

$$\frac{\partial}{\partial t} n_0 = D_l \frac{\partial^2 n_0}{\partial r^2} + S \tag{11}$$

which recovers the diffusion equation.

In the case of long-time correlations with $C(t) = C_0$ being constant Eq. (9) is

$$\frac{\partial}{\partial t} n_0 = C_0 \frac{\partial^2 n_0}{\partial r^2} \int_0^t dt' + S. \tag{12}$$

Differentiating with respect to t provides a wave equation

$$\frac{\partial^2}{\partial t^2} n_0 = C_0 \frac{\partial^2 n_0}{\partial r^2} \tag{13}$$

with the coefficient $[C_0] = m^2/s^2$. We assumed the sources and sinks being constant in time, otherwise $\partial S/\partial t$ has to be added. This equation describes super-diffusion. As a hyperbolic equation it can describe nonlocal effects.

Telegraph equation

The auto-correlation function of the fluctuations in the SOL can be well fitted by an exponentially decaying function as shown for example in TCV [28], JET [29] and COMPASS [30]. The exponential correlation function is given by

$$C(t) = C_0 \exp(-|t|/\tau) \tag{14}$$

which inserted into (9) yields

$$\frac{\partial}{\partial t} n_0 = \int_0^t C_0 \exp(-|t - t'|/\tau) \frac{\partial^2 n_0}{\partial r^2} dt' + S \tag{15}$$

Differentiating this equation with respect to t yields

$$\frac{\partial^2}{\partial t^2} n_0 = -\frac{1}{\tau} \int_0^t C_0 \exp(-|t - t'|/\tau) \frac{\partial^2 n_0}{\partial r^2} dt' + C_0 \frac{\partial^2 n_0}{\partial r^2} \tag{16}$$

where it is assumed that the background $\frac{\partial^2 n_0}{\partial r^2}$ and the sources and sinks S are rather constant within the time τ. The second term on the r.h.s. comes from the upper boundary of the integral (Leibniz integral rule) $C_0 \exp(-|t-t|/\tau) \frac{\partial^2 n_0}{\partial r^2} \frac{\mathrm{d}}{\mathrm{d}t} t$. Eliminating the integral in (15) by substituting

$$\int_0^t C_0 \exp(-|t - t'|/\tau) \frac{\partial^2 n_0}{\partial r^2} dt' = -\tau \frac{\partial^2}{\partial t^2} n_0 + \tau C_0 \frac{\partial^2 n_0}{\partial r^2}. \tag{17}$$

yields

$$\frac{\partial}{\partial t} n_0 + \tau \frac{\partial^2}{\partial t^2} n_0 = \tau C_0 \frac{\partial^2 n_0}{\partial r^2} + S \tag{18}$$

which is the telegraph equation. The telegraph equation has been used before to study nonlocal heat transport in the core of fusion plasmas [31–33] and zonal flow propagation [34]. With respect to heat transport the telegraph equation is also called Cattaneo equation. If sources and sinks depend on time a term $\tau \frac{\partial S}{\partial t}$ have to be added to Eq. (18). As no significant effects of neutrals on the blob dynamics is expected [35], this term will be neglected in the following.

Compared to the diffusion equation (11), the term $\tau \frac{\partial^2}{\partial t^2} n_0$ corresponds physically to the response time of the flux to the gradient. In the case of diffusion the transport is directly related to the gradient $\Gamma = -D \frac{\partial n_0}{\partial r}$, which corresponds to an infinitely rapid response. By introducing a finite response time $\Gamma = -D \frac{\partial n_0}{\partial r} - \tau \frac{\partial \Gamma}{\partial t}$ the density evolution is given by

$$\frac{\partial n_0}{\partial t} = -\frac{\partial \Gamma}{\partial r} = D \frac{\partial^2 n_0}{\partial r^2} + \tau \frac{\partial}{\partial r} \frac{\partial \Gamma}{\partial t}. \tag{19}$$

From $\frac{\partial n_0}{\partial t} = -\frac{\partial \Gamma}{\partial r}$ follows $\frac{\partial}{\partial r} \frac{\partial \Gamma}{\partial t} = \frac{\partial^2 n_0}{\partial t^2}$ which can be substituted for the last term in Eq. (19) to recover Eq. (18).

The telegraph equation shows different behavior on different time scales [36]. On long time scales ($t \gg \tau$) the telegraph equation (18) reduces to the diffusion equation. The effective diffusion coefficient is $D_{tele} = \tau C_0$. The correlation coefficient is $C_0 = \tilde{u}_r^2$ (see Eq. (8)). On short time scales ($t \ll \tau$) the telegraph equation shows wave-like behavior. It can describe nonlocal transport. The telegraph equation (18) can be also written as

$$\frac{\partial^2}{\partial t^2} n_0 + \frac{1}{\tau} \frac{\partial}{\partial t} n_0 = C_0 \frac{\partial^2 n_0}{\partial r^2}. \tag{20}$$

Compared to the wave equation (13) the propagation velocity is $\sqrt{C_0} = \tilde{u}_r$, which is the typical radial velocity of the fluctuations.

Illustration of the dynamics of the telegraph equation

One dimensional simulations of the telegraph equations have been carried out in simplified geometry with a finite difference upwind scheme to illustrate its dynamics. Von Neumann boundary conditions have been used, where the boundary conditions have been optimized to reduce the effects of the boundary on the main domain. The parameters have been

adapted to typical mid-SOL conditions ($T_e = 15$ eV, $L_\parallel = 20$ m, deuterium ions) in the sheath dissipative regime of blob propagation. An auto-correlation time of $\tau = 20$ μs with a blob velocity of $u_b = 250$ m/s have been used, corresponding to an analytical gradient fall-off length of $\lambda_n = 3.1$ cm. To mimic the intermittency of the SOL transport, the source of a Gaussian shape in radial direction and in time at the separatrix is randomly activated with an exponentially distributed waiting time distribution. The simulation result is shown in Fig. 2. This is similar to the stochastic framework developed in Refs. [37, 38]. In Ref. [37] one point in space is described by an uncorrelated train of pulses. These pulses are ejected in time following a Poisson process with an exponential distribution of amplitudes. The model [37] captures the non-Gaussian features of the probability distribution function well. In Ref. [38] the spatial profile in the SOL is related to the dynamics of filaments based on a statistical description of filamentary motion. We make the same distinction between background and profile as done in Ref. [38]. The background is the environment the fluctuations propagate in, which is not the same as the profile. The profile is given by the time average of the thermodynamic quantity (in this case the density), consisting of the combined background and average of the filaments. The pulses ballistically propagate through the domain. The propagation velocity is exactly the predefined radial blob velocity (Fig. 3). During propagation the pulses decay in time due the parallel drainage of the blobs. Here, there is basically no background, the resulting profile is essentially composed only of the filaments.

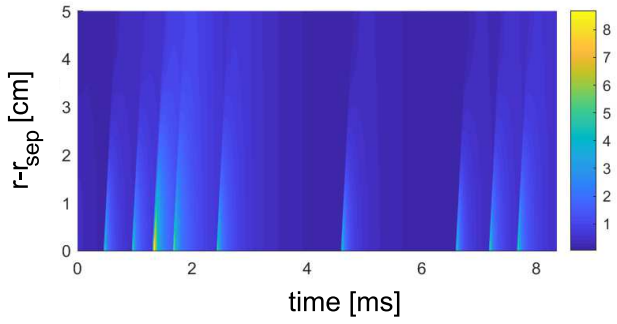

FIG. 2: Density evolution (in 10^{19} m^{-3}) simulated the telegraph equation. The source is stochasticity activated leading to pulses propagating ballistically through the domain.

The time averaged profile of the simulation is shown in Fig. 4. Even though the dynamics is nonlocal and ballistic, therefore not diffusive at all, the resulting gradient fall-off length

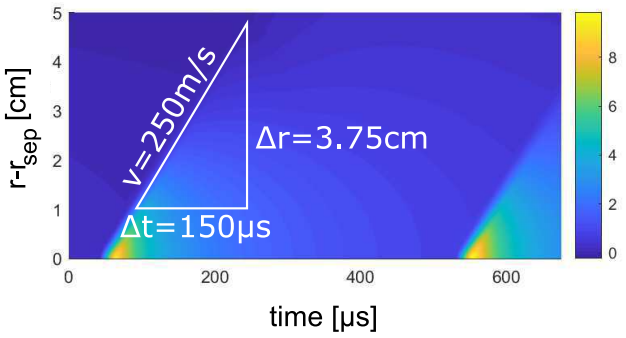

FIG. 3: Temporal magnification of pulse propagation as shown in Fig. 2. The pulse propagation is constant across the radius and thus can be directly restructured.

of the profile (not the background) agrees very well with the analytically calculated one $\lambda_n = \sqrt{DL_\parallel/c_s}$ with the effective diffusion coefficient of $D = \tau u_b^2$. Therefore it captures the ratio of the time scales of the perpendicular and parallel dynamics quite well.

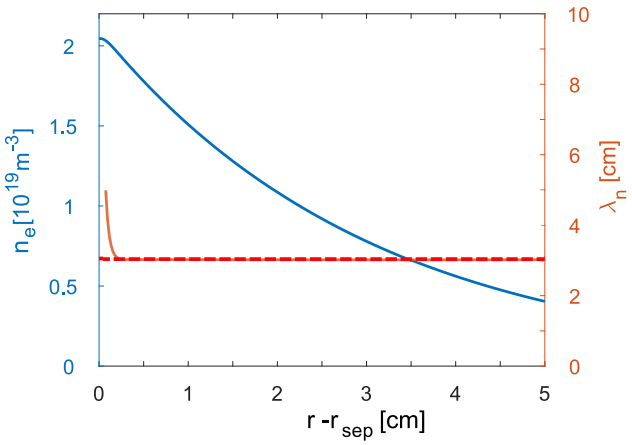

FIG. 4: Time averaged profile (shown in blue solid) and gradient scale length (shown in orange solid) of the simulation results. The time averaged profile agrees with the analytical solution (shown by the dashed red line) using an effective diffusion coefficient.

EFFECTIVE FILAMENT DIFFUSION COEFFICIENT FOR THE SOL

Order of magnitude estimate

In the telegraph-type transport model, the effective diffusion coefficient on the large time scale results from a correlated random walk. The underlying microscopic mechanism is based on super-diffusive, ballistically propagating structures with a typical radial velocity appearing on a short typical time scale. Such a picture is consistent with the SOL observation. It also provides a reasonable order of magnitude estimate. Typical radial velocities in the SOL are in the order of 10^2–10^3 m/s, typical correlation times in the order of 10 μs. This corresponds to typical SOL diffusion coefficients in the order of 0.1–10 m^2/s which are also in the typical range used in transport codes. In general the radial velocity and auto-correlation time estimated by the auto-correlation of the radial velocity fluctuations should be used. A decomposition in filaments and turbulence without filaments should not be done. However, it can be assumed that the filaments will determine the auto-correlation function. In such a case approximating the typical radial velocity by the filament velocity $\tilde{u}_r \approx u_b$ and the typical time scale by $\tau \approx \delta_b/u_b$ seem reasonable approximations. This results in an effective diffusion coefficient of $D_{\mathrm{tele}} = u_b\delta_b$. In the typical sheath connected regime appearing in attached conditions the blob velocity is predicted to decrease with the blob size $u_b \sim \delta_b^{-2}$ [7], hence $D_{\mathrm{tele}} \sim \delta_b^{-1}$. As the temperature does radially not change much in the SOL the typical blob size δ_b does not change much either, the typical effective diffusion coefficient is around $D_{\mathrm{tele}} = 1\ \mathrm{m}^2/\mathrm{s}$ for typical blobs of about $\delta_b = 1$ cm with a radial velocity of $u_b = 100$ m/s. In the inertial regime $u_b \sim \sqrt{\delta_b}$ hence $D_{\mathrm{tele}} \sim \delta_b^{3/2}$. Here we observed blobs with sizes up to $\delta_b = 8$ cm with velocities up to $v_b = 800$ m/s (not at the same time) and corresponding effective diffusion coefficients up to $D_{\mathrm{tele}} \approx 50\ \mathrm{m}^2/\mathrm{s}$. Therefore, filamentary transport, interpreted as the stationary limit given by an effective diffusion coefficient of $D_{\mathrm{tele}} = u_b^2\tau$, can account for the factor of 20 observed in density ramp-up experiments.

Example for transport code simulations

Next an example of an application is shown. ASDEX Upgrade conditions are simulated using the code SOLPS-ITER [12]. The procedure is similar to the one published in Ref. [39]. Two cases are considered, one at low density and one with the characteristic density shoulder

at elevated density. In SOLPS-ITER the diffusion coefficient D has to be set manually. This has been done for a first guess. The simulation provides the particle transport $\Gamma_{\mathrm{SOLPS}} = D(\mathrm{d}n/\mathrm{d}r)_{\mathrm{SOLPS}}$ and the profile $(\mathrm{d}n/\mathrm{d}r)_{\mathrm{SOLPS}}$, which may differ from the experimental profile. To match the simulated and experimental profile an iterative scheme has been applied. For the next step $i+1$ the diffusion coefficient at every radial location has been set to $D_{i+1} = -\frac{\Gamma_{\mathrm{SOLPS},i}}{(\mathrm{d}n/\mathrm{d}r)_{\mathrm{exp}}}$. The procedure required only a few steps until it converges to the experimental profile. These are shown in Fig. 5. The corresponding particle diffusion coefficients D are around the order of one m^2/s in the case of low density, where D increases from 0.4 m^2/s to above one m^2/s across the SOL (Fig. 5a). At elevated densities the particle diffusion coefficient is much higher, in particular around the density shoulder it approaches $D = 40$ m^2/s (Fig. 5b). In the low density case the auto correlation times τ have been measured between 10 and 50 μs, which would correspond to blob velocities $v_b = \sqrt{D/\tau}$ between 100 and 200 m/s. In the high density case the auto correlation time scatters between 50 and 250 μs corresponding to blob velocities between 400 and 900 m/s. These values are in reasonable agreement with the ones reported in literature [19].

SUMMARY AND CONCLUSION

Due to plasma filaments or blobs the transport in the scrape-off layer of tokamaks is not diffusive. It is intermittent, showing a strongly non-Gaussian distribution. It can also not be parametrized (even locally) by diffusion and convection [41]. Turbulent transport is non-local [10], which means the transport is not a function of the local quantities at a given position but depends on the quantities at a different radial position. Transport codes approximating turbulent transport via effective diffusion or convection intrinsically can not treat turbulent transport self-consistently. But transport codes include the complex magnetic geometry, neutral and impurity physics, radiation from excited states, wall recombination or even atomic and molecular chemistry. Codes treating the turbulence self-consistently usually do not treat these effects very well. Codes like GRILLIX [42] are currently in development to close this gap. Another possibility is to extend transport codes by reduced models of turbulent transport [43, 44]. For the time being effects of complex magnetic geometry, neutral and impurity physics are of fundamental importance for divertor physics and can only be studied by transport codes. The present contribution should guide the treatment of

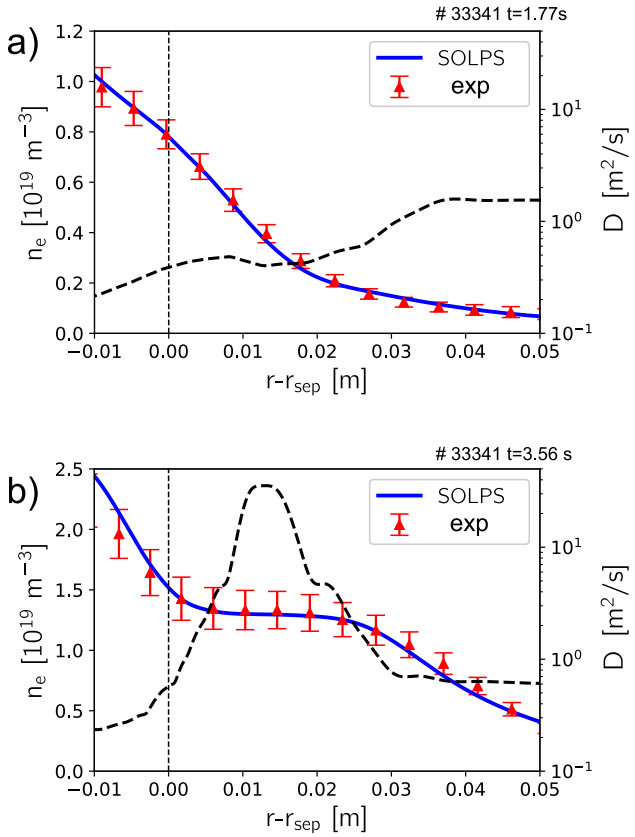

FIG. 5: Density profiles (blue solid lines) simulated by means of SOLPS-ITER of a low (a) and high density (b) case measured in ASDEX Upgrade. The experimental data points shown by the red triangles are obtained from the integrated data analysis IDA [40]. The simulated diffusion coefficients are shown by the black dashed line.

turbulent transport in the current implementation of such transport codes.

If SOL turbulence must be described by a diffusion coefficient, what would be the best way to describe it? Here, it is proposed to use the typical velocity u_b and correlation time τ of the plasma filaments in the scrape-off layer to estimate the effective diffusion coefficient $D = u_b^2\tau$. These quantities are often directly available from the experiment and be used as an input in the transport code. This effective diffusion coefficient is the diffusive limit of ballistic transport modeled by the telegraph equation, describing a correlated random walk with exponential correlation function (also a feature of SOL transport). The effective diffusion coefficient is based on the auto-correlation function and therefore it is an intrinsic statistical quantity. The transport corresponds to the averaged filamentary transport. It

is only valid for time scales much larger than the auto-correlation time, therefore it can be used for stationary solutions of the transport code, but not to study the impact of individual filaments. Using the typical blob velocity u_b and size δ_b to define a characteristic time δ_b/u_b and using these to determine a characteristic blob diffusion coefficient

$$D = \delta_b^2/\tau = \delta_b^2/(\delta_b/u_b) = u_b\delta_b = u_b^2(\delta_b/u_b) = u_b^2\tau \tag{21}$$

provides the same result if the auto correlation time is equal to this characteristic time $\tau = \delta_b/u_b$ (blob correspondence principle).

Most of the important physical effects are now hidden in these characteristic quantities (u_b, τ, δ_b), which can be deduced from theoretical models [7, 8, 45] or directly from experimental measurements [46, 47]. Blob velocity and auto-correlation time change strongly with the divertor conditions [17, 19]. The models [7, 8, 45] or measurements [46, 47] describe the blob dynamics at the outboard midplane, which is expected to have the strongest contribution to the blob induced perpendicular transport. A higher degree of sophistication is possible. The blob dynamics strongly depends on the magnetic curvature [7, 8, 45], which varies with the ballooning (roughly the poloidal) angle. The influence of the varying magnetic geometry with the ballooning angle on the blob dynamics has been investigated in Ref. [48]. Simulations of the filament motion in realistic tokamak geometry can be found in Ref. [49]. The impact of the X-point on the blob dynamics has been studied in Ref. [50]. Therefore, the models can provide the characteristic quantities (u_b, τ, δ_b) and therefore also the corresponding diffusion coefficient $D = u_b^2\tau$ even on the full 2D or 3D grid.

Acknowledgements

This work has been carried out within the framework of the EUROfusion Consortium and has received funding from the Euratom research and training programme 2014-2018 and 2019-2020 under grant agreement No 633053. The views and opinions expressed herein do not necessarily reflect those of the European Commission.

[1] H. J. Sun, E. Wolfrum, T. Eich, B. Kurzan, S. Potzel, U. Stroth, and the ASDEX Upgrade Team, Plasma Phys. & Controlled Fusion **57**, 125011 (2015).

[2] J. Boedo, D. Rudakov, R. Moyer, S. Krasheninnikov, D. Whyte, G. McKee, G. Tynan, M. Schaffer, P. Stangeby, P. West, et al., Phys. Plasmas **8**, 4826 (2001).

[3] G. Y. Antar, G. Counsell, Y. Yang, and P. Devynck, Phys. Plasmas **10**, 419 (2003).

[4] Y. H. Xu, S. Jachmich, and R. R. Weynats, Plasma Phys. & Controlled Fusion **47**, 1841 (2005).

[5] J. Cheng, L. Yan, W. Hong, T. Lan, J. Qian, A. Liu, H. Zhao, Y. Liu, Q. Yang, J. Dong, et al., Plasma Phys. & Controlled Fusion **52**, 055003 (2010).

[6] O. Grulke, J. L. Terry, B. LaBombard, and S. J. Zweben, Phys. Plasmas **13**, 012306 (2006).

[7] S. Krasheninnikov, Phys. Lett. A **283**, 368 (2001).

[8] O. E. Garcia, J. Horacek, R. A. Pitts, A. H. Nielsen, W. Fundamenski, J. P. Graves, V. Naulin, and J. J. Rasmussen, Plasma Physics and Controlled Fusion **48**, L1 (2006).

[9] P. Ghendrih, Y. Sarazin, G. Ciraolo, G. Darmet, X. Garbet, V. Grangirand, P. Tamain, S. Benkadda, and P. Beyer, J. Nucl. Mat. **363-365**, 581 (2007).

[10] P. Manz, T. T. Ribeiro, B. D. Scott, G. Birkenmeier, D. Carralero, G. Fuchert, H. W. Müller, S. H. Müller, U. Stroth, and E. Wolfrum, Phys. Plasmas **22**, 022308 (2015).

[11] X. Bonnin, J. Nucl. Mat. **390-391**, 274 (2009).

[12] S. Wiesen, D. Reiter, V. Kotov, M. Baelmans, W. Dekeyser, A. Kukushkin, S. Lisgo, R. Pitts, V. Rozhansky, G. Saibene, et al., Journal of Nuclear Materials **463**, 480 (2015).

[13] R. Simonini, Contr. Plasma Phys. **34**, 368 (1994).

[14] Y. Feng, Contr. Plasma Phys. **44**, 25 (2004).

[15] T. D. Rogulion, J. Nucl. Mat. **196**, 347 (1992).

[16] H. Bufferand, J. Nucl. Mat. **438**, 445 (2013).

[17] D. Carralero, P. Manz, L. Aho-Mantila, G. Birkenmeier, M. Brix, H. W. Müller, U. Stroth, N. Vianello, E. Wolfrum, and the ASDEX Upgrade Team, Phys. Rev. Lett. **115**, 215002 (2015).

[18] T. Lunt, D. Carralero, Y. Feng, G. Birkenmeier, H. W. Müller, S. Müller, M. Wischermeier, and the ASDEX Upgrade Team, J. Nucl. Mat. **463**, 744 (2015).

[19] D. Carralero, G. Birkenmeier, H. W. Müller, P. Manz, P. deMarne, S. Müller, F. Reimhold, U. Stroth, M. Wischmeier, E. Wolfrum, et al., Nucl. Fusion **54**, 123005 (2014).

[20] G. Birkenmeier, P. Manz, D. Carralero, F. M. Laggner, G. Fuchert, K. Krieger, H. Maier, F. Reimold, K. Schmid, R. Dux, et al., Nucl. Fusion **55**, 033018 (2015).

[21] N. Fedorczak, J. P. Gunn, N. Nace, A. Gallo, C. Baudoin, H. Bufferand, G. Ciraolo, T. Eich, P. Ghendrih, and P. Tamain, Nucl. Mat. and Energy **12**, 838 (2017).

[22] L. F. Richardson, Proc. Roy. Soc. London A **110**, 709 (1926).

[23] R. Metzler and J. Klafter, Physics Reports **339**, 1 (2000).

[24] D. del Castillo-Negrete, B. A. Carreras, and V. E. Lynch, Phys. Rev. Lett. **94**, 065003 (2005).

[25] T. Hauff, F. Jenko, and S. Eule, Physics of Plasmas **14**, 102316 (2007).

[26] R. Sánchez, D. E. Newman, J.-N. Leboeuf, V. K. Decyk, and B. A. Carreras, Phys. Rev. Lett. **101**, 205002 (2008).

[27] O. G. Bakunin, *Turbulence and Diffusion, Scaling Versus Equations* (Springer, Berlin, Heidelberg, 2008).

[28] A. Theodorsen, O. E. Garcia, J. Horacek, R. Kube, and R. A. Pitts, Plasma Physics and Controlled Fusion **58**, 044006 (2016).

[29] N. R. Walkden, A. Wynn, F. Militello, B. Lipschultz, G. Matthews, C. Guillemaut, J. Harrison, and D. M. and, Plasma Physics and Controlled Fusion **59**, 085009 (2017).

[30] A. Bencze, M. Berta, A. Burzas, P. Hacek, J. Krbec, M. Szutyanyi, and the COMPASS Team, Plasma Phys. & Controlled Fusion **61**, 085014 (2019).

[31] Ö. D. Gürcan, P. H. Diamond, X. Garbet, V. Berionni, G. Dif-Pradalier, P. Hennequin, P. Morel, Y. Kosuga, and L. Vermare, Physics of Plasmas **20**, 022307 (2013).

[32] Y. Kosuga, P. H. Diamond, G. Dif-Pradalier, and O. D. Gürcan, Physics of Plasmas **21**, 055701 (2014).

[33] S. Inagaki, K. Itoh, S.-I. Itoh, Y. Kosuga, M. Lesur, and N. Kasuya, Plasma and Fusion Research **10**, 1203002 (2015).

[34] Z. B. Guo, P. H. Diamond, Y. Kosuga, and O. D. Gürcan, Phys. Rev. E **89**, 041101 (2014).

[35] D. Schwörer, N. Walkden, H. Leggate, B. Dudson, F. Militello, T. Downes, and M. Turner, Nuclear Materials and Energy **12**, 825 (2017).

[36] A. Compte and R. Metzler, J. Physics A **30**, 7277 (1997).

[37] O. E. Garcia, Phys. Rev. Lett. **108**, 265001 (2012).

[38] F. Militello and J. T. Omotani, Plasma Phys. & Controlled Fusion **58**, 125004 (2016).

[39] J. Canik, R. Maingi, V. Soukhanovskii, R. Bell, H. Kugel, B. LeBlanc, and T. Osborne, Journal of Nuclear Materials **415**, S409 (2011).

[40] R. Fischer, C. J. Fuchs, B. Kurzan, W. Suttrop, E. Wolfrum, and A. U. Team, Fusion Science

and Technology **58**, 675 (2010).

[41] V. Naulin, Journal of Nuclear Materials **363-365**, 24 (2007).

[42] A. Stegmeir, A. Ross, T. Body, M. Francisquez, W. Zholobenko, D. Coster, O. Maj, P. Manz, F. Jenko, B. N. Rogers, et al., Physics of Plasmas **26**, 052517 (2019).

[43] H. Bufferand, G. Ciraolo, P. Ghendrih, Y. Marandet, J. Bucalossi, C. Colin, N. Fedorczak, D. Galassi, J. Gunn, R. Leybros, et al., Contributions to Plasma Physics **56**, 555 (2016).

[44] S. Baschetti, H. Bufferand, G. Ciraolo, N. Fedorczak, P. Ghendrih, P. Tamain, and E. Serre, Nuclear Materials and Energy **19**, 200 (2019).

[45] P. Manz, D. Carralero, G. Birkenmeier, H. W. Müller, S. H. Müller, G. Fuchert, B. D. Scott, and U. Stroth, Phys. Plasmas **20**, 102307 (2013).

[46] G. Birkenmeier, F. M. Laggner, M. Willensdorfer, T. Kobayashi, P. Manz, E. Wolfrum, D. Carralero, R. Fischer, B. Sieglin, G. Fuchert, et al., Plasma Phys. & Controlled Fusion **56**, 075019 (2014).

[47] G. Fuchert, G. Birkenmeier, D. Carralero, T. Lunt, P. Manz, H. W. Müller, B. Nold, M. Ramisch, V. Rohde, U. Stroth, et al., Plasma Phys. & Controlled Fusion **56**, 125001 (2014).

[48] S. Garland, G. Fuchert, M. Ramisch, and T. Hirth, Plasma Phys. & Controlled Fusion **58**, 044012 (2016).

[49] N. R. Walkden, B. D. Dudson, L. Easy, G. Fishpool, and J. T. Omotani, Nucl. Fusion **55**, 113022 (2015).

[50] F. Avino, A. Fasoli, I. Furno, P. Ricci, and C. Theiler, Phys. Rev. Lett. **116**, 105001 (2016).